

Residual stresses in as-manufactured TRISO Coated Particle Fuel (CPF)

Angelo Battistini^a, Thomas A. Haynes^{a,b}, Daniel Shepherd^c, Mark R. Wenman^{a,*}

^a Imperial College London, Centre for Nuclear Engineering, South Kensington Campus, London SW7 2AZ, UK

^b University of East Anglia, Norwich Research Park, Norwich, Norfolk, NR4 7TJ, UK

^c National Nuclear Laboratory, Preston Laboratory, Springfields, Salwick, Preston, Lancashire, PR4 0XJ, UK

ARTICLE INFO

Keywords:

TRISO Coated Particle Fuel (TRISO CPF)
Residual Stresses
High Temperature Gas Reactor (HTGR)
ABAQUS
Advanced Technology Fuels (ATF)
Advanced Modular Reactor (AMR)

ABSTRACT

TRistructural ISotropic coated particle fuels (TRISO CPF) have been developed as a possible fuel solution for high temperature nuclear reactors, which offer the possibility of nuclear cogeneration-powered industrial facilities and hydrogen production. A finite element model was developed to simulate the fabrication process of TRISO particles. Understanding the initial stress and bonding state of the layers is crucial in predicting performance and failure in service, however this factor has not received an in depth consideration in the available literature. The simulations of a fully bonded model of TRISO (layers perfectly attached to each other) revealed the presence of high values of tensile hoop stresses in the inner fuel kernel (up to 250 MPa, sufficient to cause fracture in UO_2) and even higher compressive stresses (up to 600 MPa) in the silicon carbide layer. Simulations conducted without bonding between kernel and buffer found the residual stress state to be consistently more relaxed with respect to the fully bonded model. This was most evident in the radial stress, which drops to less than 10 MPa (tensile or compressive) throughout the particle. In the hoop direction, compression of 150 MPa remained in the SiC layer. Such results are consistent with the empirical evidence of the occurrence of kernel-buffer debonding during the fabrication of TRISO particles. Finally, a brief investigation of the effect of ovality on the model with kernel-buffer debonding showed an overall increase in the magnitude of the hoop stress in the SiC and PyC layers in a flat spot caused by reduced buffer material.

1. Introduction

TRistructural ISotropic coated particle fuel (CPF) is one of the most studied and researched advanced technology fuels, with its development in the Dragon project from 1957 [1]. CPF can also be considered as accident tolerant fuels, considered to increase safety in accident scenarios [2,3]. With the deployment of advanced technology fuels, greater burnups, temperatures, efficiencies and additional economic advantages are targeted in addition to the presence of inherent safety features [4–7].

TRISO particles have been used in various prototype designs in several countries, especially for high temperature gas-cooled reactors (HTGR also known as HTR). Examples of their adoption can be found in the Thorium High Temperature Reactor (THTR-300, Germany) [8], the Chinese HTR-10 [9], the Japanese HTTR [10] and the Fort Saint Vrain Gas Cooled Reactor in the USA [11]. HTGRs are being investigated for their potential to deliver non-electricity energy supply, most notably process heat and hydrogen generation. To deliver on these applications,

much higher core outlet temperatures are delivered in HTGRs than in light water reactors (LWR). Traditional pin-type fuels (i.e., pellet in metallic cladding) are therefore not appropriate, and TRISO CPF are required. CPF have also been proposed for use in molten salt-cooled reactors, such as the fluoride-salt-cooled high temperature reactor developed by Kairos Power [12]. Several recent state-funded and private modular reactor designs make use of CPF, including the U-Battery micro-reactor, one of the advanced modular reactor (AMR) projects currently ongoing in the UK [13], Framatome's SC-HTGR [14], the recently built Chinese HTR-PM [15] and the project for the U.S. based Xe-100 modular HTGR developed by X-energy [16].

TRISO fuel is a layered spherical particle incorporating three types of coating material, with typically a UO_2 or UCO (UO_2/UC_2 mixed phase) kernel and multiple layers of protective materials enclosing it (the first designs, BISO particles, used two types of coating material, but were abandoned in their then form as their fission product retention performance was poor [17]).

The most typical layers found in TRISO are shown in Fig. 1. A porous

* Corresponding author.

E-mail address: m.wenman@imperial.ac.uk (M.R. Wenman).

<https://doi.org/10.1016/j.jnucmat.2023.154659>

Received 26 April 2023; Received in revised form 27 July 2023; Accepted 28 July 2023

Available online 29 July 2023

0022-3115/© 2023 The Author(s). Published by Elsevier B.V. This is an open access article under the CC BY license (<http://creativecommons.org/licenses/by/4.0/>).

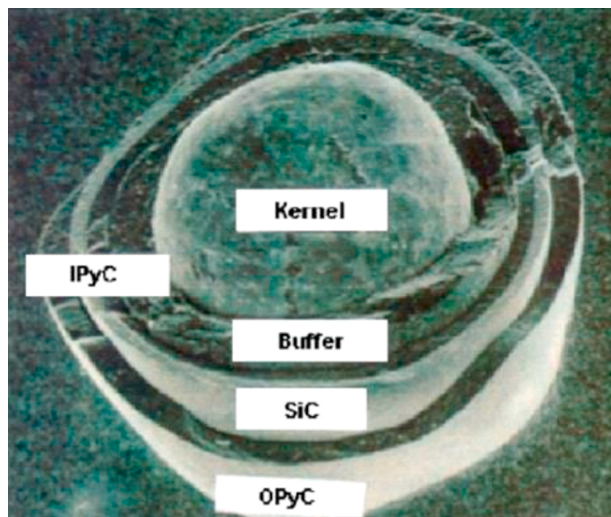


Fig. 1. Micrograph of a TRISO particle. Reproduced from [20].

pyrolytic carbon layer acts as a buffer accommodating the swelling of the kernel and the absorption of the recoil energy from fission products. Then, an inner dense pyrolytic carbon (IPyC) layer protects the outer layers from the corrosion from some of the fission products. A silicon carbide (SiC) layer provides mechanical strength to the particle, acting as a pressure vessel for the gaseous fission products and, finally, an outer dense pyrolytic carbon (OPyC) layer separates and protects the SiC layer from the outer matrix, typically graphite, in which TRISO particles are embedded [18,19].

Table 1 and Fig. 2 give the principal material properties measured for fabricated TRISO particles. Fig. 2 shows that a key aspect to consider for the structural integrity of TRISO particles is the very different thermal expansion coefficients of the materials, which are confined together in a very small space in contact or even bonded. This will give rise to thermal stresses when the temperature of the particle changes significantly

Table 1

Thermo-mechanical properties of the materials typically used in TRISO particles. The values for typical operating temperatures were calculated with the expressions contained in the referenced sources. Room temperature (RT) is assumed to be 298. 2223 K was the final manufacturing thermal treatment temperature used for the German AVR TRISO particles [21]. Density values are reported both as absolute values and as percentage of the theoretical density of the corresponding material.

Material	UO ₂	Buffer PyC	Dense PyC (IPyC, OPyC)	SiC
Elastic Modulus (GPa)	220 (RT) 172 (2223 K) [22]	11.1 (At 56% porosity) [23]	17.9 (At 16% porosity) [24], [25]	451.4 (RT) 394.2 (2223 K) [26]
Poisson's Ratio	0.32 [27]	0.23 [23]	0.33 [28]	0.21 [29]
Coefficient of Thermal Expansion (CTE) (10 ⁻⁶ K ⁻¹)	9.8 (RT) 19.1 (2223 K) [23]	3.5 [23]	5.5 [23]	2.2 (RT) 5.0 (T > 1273 K) [29]
Density (kg m ⁻³) [17]	1.1 × 10 ⁴ (99% of theoretical density in [30])	9.9 × 10 ² (44% of theoretical density in [31])	1.9 × 10 ³ (84% of theoretical density in [31])	3.2 × 10 ³ (99.5% of theoretical density in [29])
Conductivity (W m ⁻¹ K ⁻¹)	8.27 (RT) 2.34 (2223 K) [32]	5.7 [33]	13.5 (IPyC) 3.4 – 4.2 (OPyC) [33]	168 [33]

during reactor operation (especially during start-up or shutdown transients), or even before fuel loading, for instance during manufacture, potentially leading to residual stresses in the as-fabricated condition.

TRISO particles are usually fabricated via successive layer chemical vapour deposition (CVD) methods [21] upon spherical fuel kernels that were formed previously by sol-gel precipitation [34]. In Table 2, a summary regarding some of the most tested designs shows how the different post sol-gel processes occur over a great span of temperatures.

The U.S. data was from the new production modular high temperature gas reactor (NP-MHTGR) project, which employed the performance test fuel produced by General Atomics (GA) and Babcock & Wilcox (B&W) [21]. German data was from the same fuel used in their HTGR and derivative designs and it was developed over the span of 30 years of research [35]. Japanese data was from the high temperature test reactor (HTTR) project; the result collaboration between the Japan Atomic Energy Research Institute (JAERI) and the Nuclear Fuel Industries (NFI), Ltd. [36]. Finally, Chinese fuel was from the demonstration high temperature reactor (HTR-10); the result of development by the Institute of Nuclear Energy Technology (INET) [37].

Table 2 shows that the manufacture of TRISO particles is not a uniform process, in particular with respect to temperatures and coating conditions. The formation of layers of different materials, with very different strengths, stiffnesses and thermal properties and the variety of temperatures involved may lead to a complex residual stress distribution in the final particle. Therefore, the production methods used could have a significant impact on the performance of the fuel during its in-service lifetime.

Historically, much importance has been given to the calculation of the stresses arising during reactor operation. Evidence of this can be found in research spanning the last four decades, which ranges across several degrees of approximation in the calculation of stresses in TRISO particles. Analytical models, such as within the UK STRESS3 [38] code or the closed form devised at Idaho National Laboratory (INL) [23,39], are very useful for implementation in 'Monte Carlo' models, in order to expedite TRISO failure probability calculations. For instance, Miller and Bennett [39] studied the local stress distribution in a 3-layer (IPyC–SiC–OPyC) TRISO shell, either intact or with partial IPyC–SiC debonding, when raised to operating temperatures while internally pressurised, and then subjected to an increasing neutron fluence. Numerical models have also been popular, especially with the recent increases in computational power available for research. Several have been developed for incorporation into finite element fuel performance codes such as BISON and PARFUME from INL [23,26,40], or ATLAS from CEA (Commissariat à l'Énergie Atomique et aux Énergies Alternatives) [23,26]. Simulations with these codes have been trying to represent many of the scenarios TRISO particles are required to withstand in a reactor, such as high neutron fluences [38,39,41], or the thermomechanical interaction of neighbouring TRISO particles inside a pebble or prismatic compact matrix [42].

One common denominator between all the aforementioned models is the starting stress distribution in the particles, which are to be considered essentially stress-free at the beginning of their simulations of reactor operation. However, there is scarcity of literature on the as-fabricated stress conditions inside TRISO particles and hence whether the stress-free assumption is appropriate. Therefore, the work reported in this present paper wishes to tackle this gap in knowledge and thus its analysis could serve as an improvement on current TRISO performance models as it would allow for greater confidence (or new insight) on the initial conditions for simulations or reactor operation, accordingly leading to higher fidelity models.

The paper begins with an overview of the finite element model (FEM) adopted for the simulations, including an analysis on how the fabrication process is approximated in the model. Following this, the residual stresses arising from fabrication of TRISO particles are reported. Results include simulations conducted on TRISO particles from the German AVR research group, which are representative of the most adopted type of

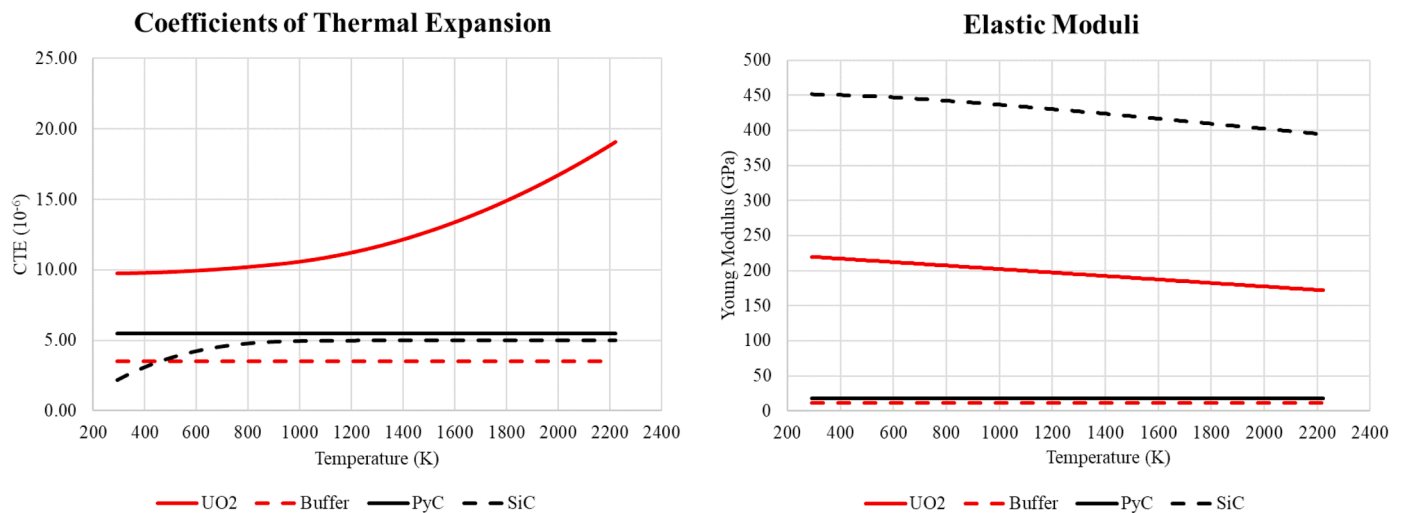


Fig. 2. Temperature dependence of the principal thermo-mechanical properties for the materials used in TRISO particles [22–24,26,29]. The reported behaviours are calculated assuming the densities mentioned in Table 1.

Table 2

Summary of the fuel kernel fabrication and coating process temperatures that have been used to make TRISO particles [21].

Country		U.S.A. (UCO)	GERMANY (UO ₂)	JAPAN UO ₂	CHINA (UO ₂)
Kernel	Drying	Air, 60 °C	80 °C	Air/H ₂ O, 200 °C	Infrared
	Calcination	Ar, 350 °C	Air, 300 °C	Unknown	Air, 500 °C
	Reduction	Ar-4%H ₂ , 1600 °C			Ar-4%H ₂ , 900 °C
	Sintering	Ar-CO, 1800 °C	H ₂ , 1600–1700 °C	Ar-4%H ₂ , 1300 °C	H ₂ , 1550 °C
Buffer	Coating Gas			Ar-C ₂ H ₂	
	Temperature	1300 °C	1250 °C	1380 °C	1100–1400 °C
IPyC	Dep. Rate/Time	Unknown	6–10 μm min ⁻¹	< 60 min	Unknown
	Coating Gas		Ar-C ₂ H ₂ -C ₃ H ₆	Ar-C ₂ H ₄	Ar-C ₂ H ₂ -C ₃ H ₆
SiC	Temperature	1230 °C	1300 °C	1380 °C	1370–1420 °C
	Dep. Rate/Time	2.2 μm min ⁻¹	4–6 μm min ⁻¹	< 60 min	Unknown
OPyC	Coating Gas		H ₂ -CH ₃ SiCl ₃		Ar-H ₂ -CH ₃ SiCl ₃
	Temperature	1650 °C	1500 °C	1600 °C	1500–1570 °C
OPyC	Dep. Rate/Time	0.2–0.4 μm min ⁻¹	0.2 μm min ⁻¹	0.1–0.4 μm min ⁻¹	60–200 min
	Coating Gas		Ar-C ₂ H ₂ -C ₃ H ₆	Ar-C ₃ H ₆	Ar-C ₂ H ₂ -C ₃ H ₆
OPyC	Temperature	>1300 °C	1300 °C	1380 °C	1370–1420 °C
	Dep. Rate/Time	< 4 μm min ⁻¹	4–6 μm min ⁻¹	< 60 min	Unknown

TRISO particles and the ones adopted for the U-Battery project. The choice of the German AVR TRISO particle is also related to the wider availability of information on the temperatures and deposition rates for the manufacturing process. Results for both a fully bonded TRISO particle where none of the layers are allowed to debond and on an analysis of the residual stress distribution for particles with kernel-buffer debonding is included. The debonded work is motivated by recent observations with x-ray micro-tomography conducted on “real” (zirconia kernels and TRISO standard coating) and “mock” (alumina kernels with non-standard coating) TRISO particles [43]. The results include the effect of a thermal annealing process known to be applied to the final fuel pebble [21], which is in place to finalise the composition of the pebble (carbonisation of the pyrolyzed resin and densification of the graphite matrix).

Finally, a brief analysis of the effect of ovality on the stresses in the debonded particle has been reported, to understand the effects of fabrication anomalies on the residual stress distribution. The thermal annealing phase was not included in the model for the debonded particles, as the stresses predicted in such particles were not judged high enough to cause any significant thermal creep.

2. Methodology

2.1. Material properties selection

Although it was eventually possible to report and use an exhaustive set of properties in a TRISO model, the data available on TRISO materials is scarce and mostly related to outdated particles and fabrication techniques. Temperature-dependant properties, for instance, are available for only some of the materials actually used in TRISO, and when they are available, they are related to different applications, e.g. certain properties of UO₂ in TRISO are assumed to be similar to those used in conventional pellet fuel (thermal conductivity, CTE, etc.) [13], but such assumptions, while being commonly relied upon, have little confirmation in literature. Moreover, the temperature dependence of PyC properties or its thermal creep behaviour are essentially missing from the literature, with only a few papers on selected values of porosity available. Such scarcity of literature should be tackled by future experimental campaigns if the level of confidence in the results from TRISO performance codes is to be increased.

The material properties adopted for this work are given in Table 1. Apart from the lack of well characterised material properties, the reason for which many of the values reported in Table 1 are given as single entries (density, specific heat and PyC properties) is that they are not likely to greatly affect the final results of the simulation, e.g. the density values do not significantly influence the thermal stress of the particle,

although they are still required for the finite element simulations to run. Moreover, due to the very small dimensions of the particles, specific heat variations over the temperature range will only weakly affect the temporal change in the temperature distribution inside the particle. Also, a simplifying assumption adopted for the simulations is instantaneous thermal equilibrium throughout the particle, which means that the specific heat in the particle layers is irrelevant to the result. Finally, as previously mentioned, PyC properties are often available only as single values in numerous literature sources [13]. Due to the combination of the presence of significant fabrication residual stresses at high temperatures, for reasonably long periods of time (especially during the annealing process), it was sensible to include thermal creep models in the simulation, to account for the stress relaxation.

2.1.1. UO₂ creep model

In the BISON finite element fuel performance code [44], creep models are derived from the ones used in MATPRO [22], which provide creep strain rates, each one describing a different phenomenon occurring in the material. In this work only the thermal creep was modelled, therefore the strain rate is implemented as follows:

$$\dot{\epsilon}_1 = \frac{C_1 \sigma e^{-\frac{Q_1}{RT}}}{(C_2 - P)G_s^2} + \frac{C_3}{C_4 - P} \sigma^{4.5} e^{-\frac{Q_2}{RT}} \quad (1)$$

Where C₁, C₂, C₃, C₄ are constants, σ is the equivalent stress in MPa, Q₁ and Q₂ are activation energies (calculated from [44] assuming that UO₂ is stoichiometric), G_s is the mean linear intercept (MLI) grain size (m), P is the fractional/decimal porosity, R is the gas constant and T is the temperature (K). The values of the parameters are reported in Table 3.

2.1.2. SiC creep model

The thermal creep strain rate in SiC has been described by a power law [46]:

$$\dot{\epsilon} = A \left(\frac{\sigma}{G}\right)^n e^{-\frac{Q}{RT}} \quad (2)$$

Where A is a constant, Q is the activation energy (J mol⁻¹), n is the power law exponent and G is the shear modulus (MPa), whose temperature dependence is given in [47], where ΔG has units of MPa K⁻¹:

$$G = G_0 - \Delta G \cdot T \quad (3)$$

Values for the parameters are reported in Table 4.

2.1.3. Buffer, iPyC, OPyC creep model

Due to the lack of information in the literature regarding the thermal creep behaviour of PyC, thermal creep in the buffer, iPyC and OPyC layers was not included but this area is highlighted to the community as an aspect where research is needed for more complete models in future.

2.2. Manufacturing process – Pre-processing

The analysis is performed using the commercial finite element code ABAQUS, which allows the coupling of mechanical effects to the thermal behaviour of the particle. For this study, the TRISO particle was modelled as an axial-symmetric semicircle, seen in Fig. 3. This is done so that a fine mesh can be used to capture any steep gradients in the stress-strain fields, which would be impractical in a 3D case, even if only a small section of the particle was analysed.

As the fabrication of the particle occurs in sequential steps, an

Table 4
Parameters for SiC creep strain rate equations [46,47].

Constant	T ≤ 1873 K	T > 1873 K
A (s ⁻¹)	71.61	1.36x10 ⁷
n	2.3	3.7
Q (J mol ⁻¹)	1.74x10 ⁵	
G ₀ (MPa)	1.6x10 ⁵	
ΔG (MPa K ⁻¹)	23	

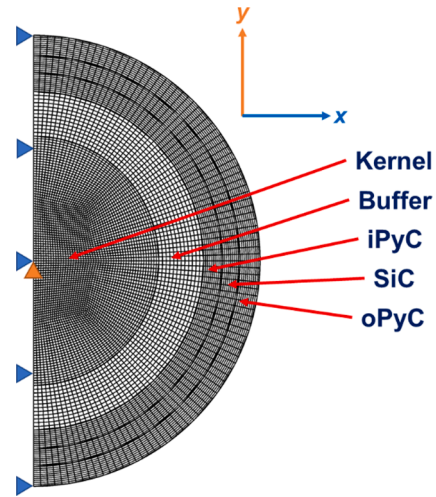


Fig. 3. Mesh adopted for the simulations. It is possible to outline the five different regions composing the TRISO particle, including kernel, buffer, inner pyrolytic carbon layer, silicon carbide layer and outer pyrolytic carbon layer.

analogous approach has been adopted to set up and run the simulations. However, as it is assumed that the available literature only provides the dimensions for TRISO particles once cool after all the coating stages have been completed, a preliminary set of reverse engineering simulations was carried out to retrieve a reasonable set of dimensions for the particles at temperature during each stage of their fabrication. These simulations can be summed up in 4 steps as detailed in Table 5 alongside the start state. The steps employ a linear temperature change over an hour time interval. This choice is arbitrary, as the models used for these preliminary simulations assume a perfectly elastic behaviour of the materials and do not take account of the elastic limits at which thermal shock could cause cracking within these brittle ceramic materials. It is also assumed that the interval is sufficiently rapid such that creep effects are negligible to the dimensional change of the particles.

A complete TRISO particle taken at room temperature is heated until it reaches the deposition temperature for the PyC layers (1573 K – step “Full Particle Reheat” in Table 5). The thickness of the OPyC layer is recorded at such temperature and assumed to be the actual thickness of the layer when it was initially deposited.

Then, a new TRISO particle model is set up without the OPyC layer. This model’s dimensions are taken from the results of step “Full Particle Reheat”, and it is heated up from 1573 K to the deposition temperature of the SiC layer (1773 K). The ‘as deposited’ thickness of the SiC layer at this elevated temperature is recorded for future use in the fabrication simulations. The successive layers are then hypothetically removed in the same way, with the temperatures and associated dimensions given in

Table 3
Parameters for UO₂ creep strain rate equations [22].

C ₁ (m ² s ⁻¹ MPa ⁻¹)	C ₂ (1)	C ₃ (s ⁻¹ MPa ^{-4.5})	C ₄ (1)	Q ₁ (J mol ⁻¹)	Q ₂ (J mol ⁻¹)	G _s (m)	P (1)
3.92x10 ⁻⁹	0.123	2.0391	9.5x10 ⁻²	3.766x10 ⁵	5.523x10 ⁵	1.3 – 1.36 x10 ⁻⁵ [45]	1.003x10 ⁻² [17]

Table 5

Dimensions of the layers of the fully bonded TRISO model at each temperature during fabrication. The as-manufactured “Start” dimensions are from [21], page 19. The dimensions for the kernel after its sol-gel formation are omitted, as the deposition of the buffer is assumed to be upon a stress-free kernel. The shaded cells indicate the values used in subsequent simulations.

Step	Temperature	Kernel radius (μm)	Buffer thickness (μm)	IPyC thickness (μm)	SiC thickness (μm)	OPyC thickness (μm)
<i>Start</i>	293 K	250.00	92.00	39.00	35.00	40.00
<i>Effect of Simulated Full Particle Reheat</i>	1573 K	253.46	91.21	39.16	35.18	40.75
<i>Effect of Simulated OPyC Removal</i>	1773 K	254.17	90.97	38.16	35.21	N/A
<i>Effect of Simulated SiC Removal</i>	1573 K	253.44	91.08	39.14	N/A	N/A
<i>Effect of Simulated IPyC Removal</i>	1523 K	253.28	91.01	N/A	N/A	N/A

Table 5.

One last step to simulate the effect of removal of the buffer layer could have been included at the end of this sequence. However, were the buffer to be hypothetically removed, the only material remaining in the particle would be the UO₂ kernel and the focus of this study was limited to residual stresses in the coating layers. For similar reasons, the model was not further developed to take account of potential residual stress that could be present in the kernel due to cooling from its sintering temperature (1873–1973 K) down to room temperature and then its subsequent heat-up for buffer deposition (to 1523 K). Such cooling is required to allow for material transfer, as deposition of the coatings would be performed in a different furnace to that used for sintering.

Each material is treated as homogenous, which would yield stress-free thermal expansion and contraction were there no interaction with the other materials. Thus, the residual stress results of the model are targeted to the separate effect of the CTE mismatch between the different materials.

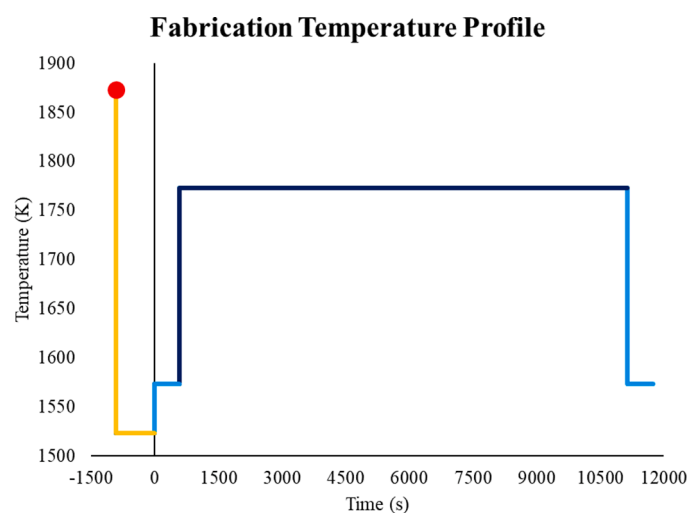


Fig. 4. Fabrication temperatures history for German AVR TRISO fuel. The yellow transient is hypothetical for the reasons of furnace material transfer discussed in the text and was not simulated as it was assumed to not to significantly influence the final stress profile of the particle coating layers. The more realistic kernel cooldown to room temperature before buffer layer deposition is not included in the Figure to avoid compressing the temperature scale in the region of interest.

2.3. Manufacturing process – Simulation campaign

The complete sequence of temperature and deposition times for the fabrication of German TRISO particles is shown in Fig. 4, with a schematic of how the TRISO layers are deposited in Fig. 5. The simulation campaign can be described by a succession of 13 steps, summed up in Table 6, which in this work are represented by four simulations run on an equal number of models, three to mimic the high temperature deposition process, and one cooldown simulation from which the majority of the residual stresses arise.

All the simulations were run on a free particle model with no pressure boundary conditions. The revolution axis of the axisymmetric model particle is fixed horizontally (x direction), and the centre of the particle is fixed vertically (y direction), as shown in Fig. 3. These constraints serve to keep the particle stationary during the transients and ensure polar and azimuthal symmetry in the particle response. A temperature boundary condition is applied on every element of the mesh (seen in Fig. 3). The general setup of the steps in the simulation campaign is described below, with a summary of the full procedure reported in Table 6.

The simulation campaign begins with a kernel and buffer model, with dimensions taken from step “IPyC Removal” of the preliminary model results (see Table 5). The initial temperature was set to 1523 K and the first transient is an almost immediate increase in temperature (through 1 second) applied to the whole particle up to the IPyC deposition temperature (1573 K). This fast increase in temperature can be adopted under the assumption that creep and thermal shock effects do not occur during the heat-up (and cool-down) sequences during fabrication, between the temperatures. For a higher fidelity fabrication model, a linear increase in temperature with the actual heating rate adopted for TRISO particles (information not available at this time but realistically around 5 – 30 K/min) would be required. The small particle size means that temperature gradients in the particle are not expected. Since the IPyC layer is continuously deposited at the final temperature of this first step, but a deposition model is not implemented for this analysis, the kernel and buffer model was kept at 1573 K for 587 s, assuming a deposition rate for the IPyC layer of $4 \mu\text{m min}^{-1}$ [21]. At the end of this step, the final stress state in the kernel and buffer and their dimensions are recorded.

A new model consisting of kernel, buffer and IPyC was then set up, with the dimensions of kernel and buffer taken from the end of the previous simulation, and the IPyC thickness retrieved from step “SiC Removal” in the preliminary simulations (See Table 5). The stress values (in kernel and buffer) from the previous simulation calculated on each of the layers’ finite elements are used as the initial values for the new simulation with kernel, buffer and IPyC. By doing this, the thermal

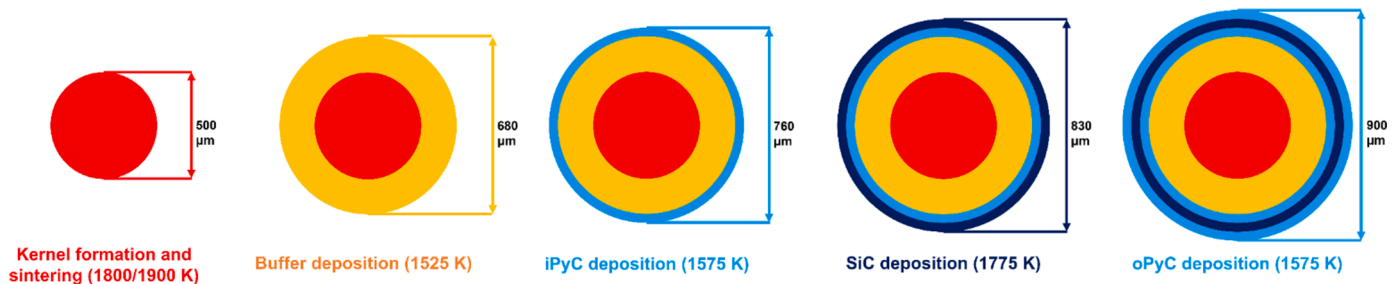


Fig. 5. Layer evolution during the fabrication of German AVR TRISO fuel. The colours of the deposited layers are the same as those used in Fig. 4.

Table 6

Deposition sequence used to determine the residual stresses. The colour code is the same used in Fig. 4 and Fig. 5. Notes: the kernel fabrication and buffer deposition were not simulated and the thermal ageing step is added after fabrication, therefore these steps and their corresponding colour coding are not included in this Table. “Thermal (Neg)” stress states refer to residual stresses arising due to the cool-down of the layer from its deposition temperature. “Low Creep” stress states refer to thermal creep effects being included in the model (for UO₂ and SiC), but due to the low temperatures and overall stress state, their effect being negligible to the residual stress in the layers.

Step	Model components	Δt (s)	Time (s)	T (K)	Stress state				
					Kernel	Buffer	IPyC	SiC	OPyC
0	K, B	N/A	0	1523	Free	Free	N/A	N/A	N/A
1	K, B	1	1	1573	Thermal	Thermal	N/A	N/A	N/A
2	K, B	587	588	1573	Thermal + Low Creep	Thermal	N/A	N/A	N/A
3	K, B, IPyC	0	588	1573	Thermal + Low Creep	Thermal	Free	N/A	N/A
4	K, B, IPyC	1	589	1773	Thermal + Low Creep	Thermal	Thermal	N/A	N/A
5	K, B, IPyC	10564	11153	1773	Thermal + Low Creep	Thermal	Thermal	N/A	N/A
6	K, B, IPyC, SiC	0	11153	1773	Thermal + Low Creep	Thermal	Thermal	Free	N/A
7	K, B, IPyC, SiC	1	11154	1573	Thermal + Low Creep	Thermal	Thermal	Thermal	N/A
8	K, B, IPyC, SiC	604	11758	1573	Thermal + Low Creep	Thermal	Thermal	Thermal (Neg) + Low Creep	N/A
9	K, B, IPyC, SiC, OPyC	0	11758	1573	Thermal + Low Creep	Thermal	Thermal	Thermal (Neg) + Low Creep	Free
10	K, B, IPyC, SiC, OPyC	7200	18958	293	Thermal (Neg) + Low Creep	Thermal (Neg)	Thermal (Neg)	Thermal (Neg) + Low Creep	Thermal (Neg)
11	K, B, IPyC, SiC, OPyC	7200	26158	2223	Thermal + Creep	Thermal	Thermal	Thermal + Creep	Thermal
12	K, B, IPyC, SiC, OPyC	1-18 hours	29758-90958	2223	Thermal + Creep	Thermal	Thermal	Thermal + Creep	Thermal
13	K, B, IPyC, SiC, OPyC	7200	36958-98158	293	Thermal (Neg) + Creep	Thermal (Neg)	Thermal (Neg)	Thermal (Neg) + Creep	Thermal (Neg)

strains arising in the next transient will change the particle’s stress state considering the history of the fabrication stresses. The stress state of the new layer (IPyC) is assumed to be null, as in the fabrication process it is deposited at a constant temperature, therefore little to no thermal stresses should arise in this layer. The procedure was then repeated two more times for the SiC and OPyC layers (Steps 6–9), with deposition times and temperatures detailed in Table 6, before the final cooling down and thermal treatment phases (Steps 10–13). The thermal treatment temperature is the same used for German AVR TRISO particles, 1950 °C (2223 K) [21], and different durations from 1 to 18 h have been modelled to investigate the effect of this parameter on the final stress state.

One of the most important approximations adopted for this work is the modelling of the interface behaviour between the layers. During fabrication, each layer is gradually deposited on the preceding layer (or kernel, in the case of the buffer). Because of the nature of fluidised bed CVD, the outer surface of each layer would have a certain degree of porosity, allowing the next vapour deposit in the fabrication process to partly infiltrate the previous surface. This interfacial region will have a

different average composition and therefore fracture tolerance, to radial or tangential tensile and compressive stresses, which may be important in determining the overall stress state of the particle during thermal transients. Experiments also show how the grain structure of the material closer to the interfaces will differ, for example smaller grains of SiC being present at the interface with IPyC compared to larger ones adjacent to the OPyC [48], with possible implications for the relative isotropy of the material properties. Due to the scarcity of literature on the effect of these features on interfacial strengths, the first model assumes infinitely strong interfaces, where the boundary nodes of each layer have their degrees of freedom “tied” to the adjacent ones. To analyse the dependence on the behaviour at the interfaces, which may be intact (completely tied) or broken (untied, only contact relationships), an additional model where the buffer layer is not tied to the kernel has also been analysed. In such a model, interpenetration between kernel and buffer is avoided with a hard-contact, no-friction model between the two layers, instead of a tie constraint.

3. Results and discussion

3.1. Fully bonded model

As shown in Fig. 6-a, immediately after the cooldown of the particle following fabrication (before the heat treatment), the radial stress in the bonded model decreases from the kernel to the OPyC external surface, with hypothetical strong tensile stresses present in the kernel of around 260 MPa. Since for this and all the successive analyses the particle has been assumed free, that is, no external pressure has been applied (which would not be the case during the compaction phase of the fuel element production), the retrieved boundary value of radial stress is consistent. The inner values should be related to the fact that the thermal expansion coefficient of UO_2 is higher than that of either PyC or SiC. This means the kernel contracts more when the temperature is decreased and therefore experiences the outer layers “pulling” towards the outside, generating a tensile radial stress state. Actual high tensile stresses (>50 MPa) in brittle ceramic materials especially UO_2 and SiC do not seem plausible without risking cracking which is not seen in actual quality assured TRISO particles. In particular, the SiC layer will ideally be in compression following manufacture to resist pressurisation from the build-up of fission gases escaping the kernel. Therefore, the buffer debonded model appeared to give more realistic results.

The hoop stress distribution (shown in Fig. 6-b) has been found to be more complicated. The residual stress in the kernel was again tensile, with a similar value (around 260 MPa) to the radial stress. This is consistent with the sphericity of the kernel, which means it is isotropic and therefore the stress state should be only dependant on the radial coordinate. Therefore, the kernel is in a state of hydrostatic tension (confirmed by the value of the second invariant, three orders of magnitude lower than the principal stresses), therefore the equivalent stress will be so low that creep and plastic effects would be minimal during fabrication. This is confirmed by the values of creep strain in the kernel at the end of the simulations, omitted for brevity purposes, which are three to four orders of magnitude lower than in the SiC layer. These conditions could be disrupted by the presence of inhomogeneities in the boundary forces acting on the kernel, such as those originated by asymmetrical or even missing layers. This possibility is important to consider when studying the effects of ovality on TRISO particles fabrication, but beyond the scope of this paper.

The outer layers, however, seem to react to the cooling contraction of the particle differently. The buffer layer is in an overall compressive hoop stress state, with stress values decreasing (in absolute value) from the kernel boundary towards the IPyC boundary, where they are almost

null. The IPyC and OPyC layers are characterised by a tensile hoop stress state, on average around 100 MPa in the IPyC (close to its fracture stress) and 25 MPa in the OPyC. Perhaps most reassuringly, the SiC layer is dominated by a compressive hoop stress state, which slightly decreases in magnitude from the inner to the outer boundary of the layer. This variation in the stress distribution is probably related to the different contraction in the hoop direction and the strong bond (tie constraint) existing at the interface between the layers. The UO_2 expansion coefficient is around 4 times larger than SiC, as per Table 1, therefore, if perfect bonding is assumed, when it cools down its circumference would reduce more than free SiC. If the interfaces cannot break and in a perfectly elastic model, this leads the SiC layer to a compressive hoop stress of around 600 MPa. This large stress is related to its higher elastic modulus (compared to PyC and UO_2) and the compound effect of PyC and UO_2 differential shrinkage.

Alongside the as-fabricated particle results, the effects of different thermal ageing treatments have been simulated for the more extreme case of the hoop stress in the bonded model. The accuracy of the results is dependant on the validity of the creep models implemented in the code, especially those for SiC, as these may not be representative due to the literature data not being optimised for behaviour at the scale of TRISO particles. Nevertheless, the results indicate that thermal ageing longer than 12 h would not significantly affect the stress conditions in the particle. This is shown in Fig. 7, in which the SiC layer residual hoop stress (the one mostly affected by the treatment) converges to around 850 MPa (compressive) after 12 h.

The effect of a prolonged time at high temperature is essentially that of enabling thermal creep to relax possible stresses occurring during the high temperature phase. This is a consequence of the change in the radial dimensions driven by the hoop stresses in the SiC layer appearing at the holding temperature. Indeed, during the heat-up phase to the thermal ageing temperature (around 400 to 600 K higher than the deposition temperatures), the stress distribution in the particle is opposite to the residual stress at room temperature, with tensile hoop stress in the SiC and buffer and compressive hoop stress in kernel and PyC layers. The thermal creep occurring at 1950 °C relaxes the tensile stresses that have arisen in the SiC (due to the lower thermal expansion coefficient of SiC with respect to UO_2 and PyC). When the particle is cooled down, however, the shrinkage thermal strain occurring in the SiC is the same for all the thermal treatment times considered (1 h, 6 h, 12 h, 18 h) because the temperature drop to room temperature is the same (~1930 °C), therefore due to the lower initial tensile stress remaining in the SiC (at 1950 °C) the final stress distribution (at room temperature) will be lower (more compressive). The same effect happens for the PyC

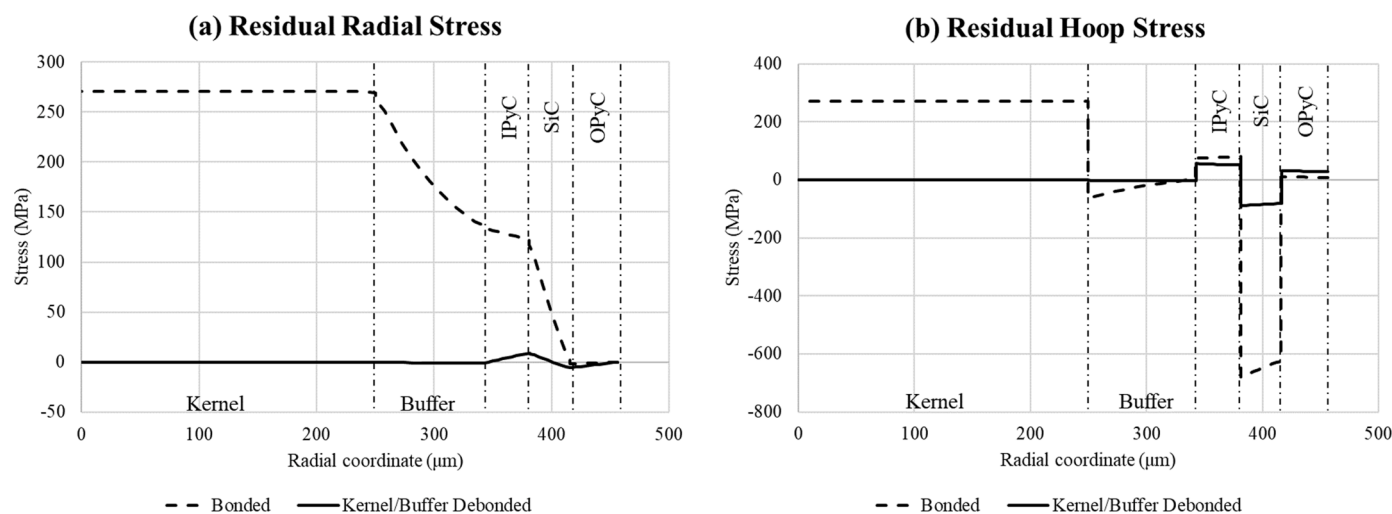


Fig. 6. Radial (a) and hoop (b) residual stresses at the end of the fabrication procedure for the German AVR TRISO particle (before the heat treatment). Comparison of the residual stress distribution between the fully bonded model and with kernel-buffer interface failure (debonded). Particle analysed at room temperature.

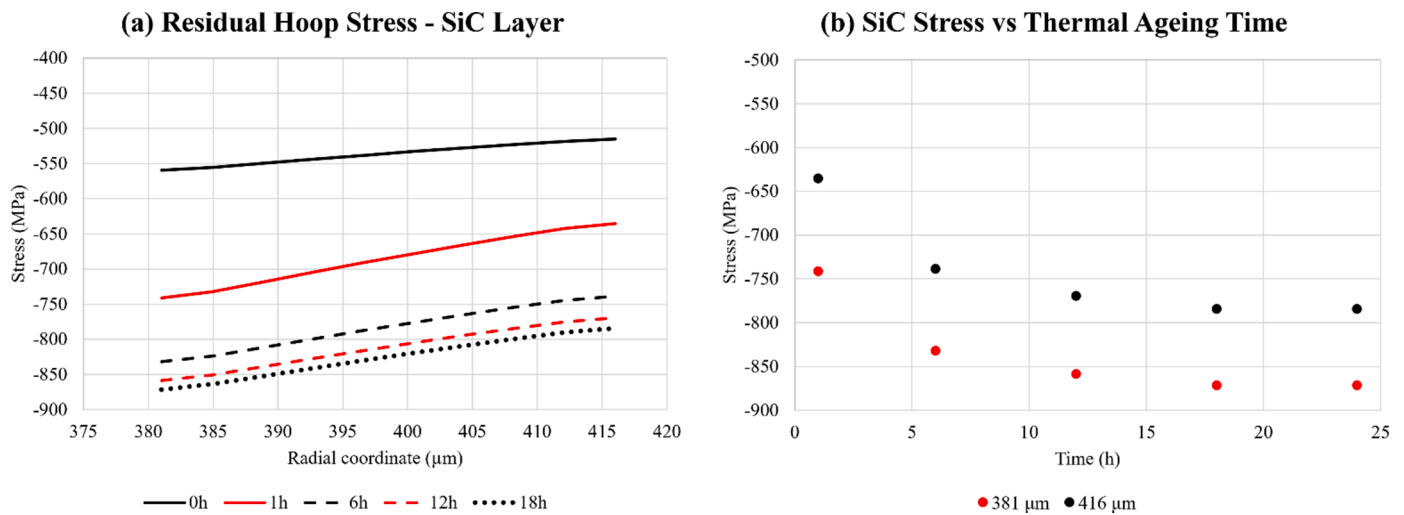


Fig. 7. (a) Residual hoop stress distribution in the SiC layer for particles undergoing different periods of thermal ageing treatment (none, 1 h, 6 h, 12 h, and 18 h at 1950 °C), (b) maximum and minimum stress in the SiC layer against thermal treatment duration (the legend refers to the radial coordinate at which the stress is reported).

layers, with lower compression remaining at high temperature and consequently higher residual tensile stresses at room temperature (as shown in Fig. 10).

This first analysis has pointed out potentially interesting information on the state of TRISO particles at the end of their production cycle but assumes no debonding between layers. When the particle is cooled down, the effect of thermal expansion coefficient mismatch in the several layers of the particle leads to a complicated but significant start-of-life residual stress profile.

3.2. Debonding hypothesis

The possibility of such high radial and hoop stresses, at the end of the fabrication cycle of the particle, led to consideration of layer debonding. One of the least convincing results of a fully bonded model is the presence of a high tensile radial stress in both kernel (260 MPa) and buffer (150–260 MPa), most notably at the boundaries between layers. Such stress is not consistent with the literature on the strength of the buffer PyC which is considered to be 40 MPa to 50 MPa [49] (median value for low-density pyrolytic carbon). These values are also not consistent with the literature value of the fracture strength of uranium dioxide in standard pellets, which is in the order of 80 MPa to 150 MPa [50,51].

Such lower fracture strength values suggest cracking in the buffer, the kernel or at the interface may occur during the fabrication process itself. At the same time, the radial tensile state of SiC found at the end of the simulation is not realistic for the adoption of TRISO fuel in a reactor, as it would affect negatively the fission product retention capability of the layer. Hence the simulation results are not plausible without the introduction of kernel debonding.

The same conclusion can be devised by the observation of several images of unirradiated TRISO particles, where there is a recurrent gap between the kernel and buffer layer, or in the buffer itself, close to the interface. In Fig. 8, showing TRISO particles with uranium dispersion from the kernel to the buffer, it is clear that partial delamination has occurred, in the spots pointed out by the red arrows. The examples are taken from defective particles due to the scarcity of literature on unirradiated flawless particles.

In Fig. 9, TRISO particles with high-Z elements infiltrations are shown. In these particles, the decoupling between kernel and buffer appears to be complete, however, as for Fig. 8, it is possible to see that the delamination can either occur between the layers (interface failure) or in the buffer (weakest material failure).

Considering this evidence, an additional set of simulations was conducted to determine the residual stress distribution in the case the

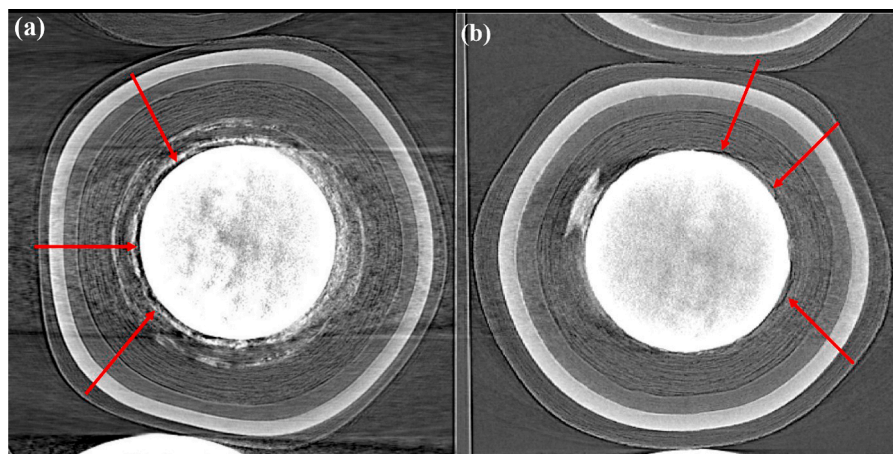


Fig. 8. X-ray microtomography images of defective unirradiated TRISO particles showing partial kernel-buffer debonding present. Reproduced from [52]. The red arrows point to the most evident delamination that has occurred between kernel and buffer. For completeness purposes, (a) shows a uniform dispersion of uranium in the buffer layer, whereas the dispersion in (b) is localised.

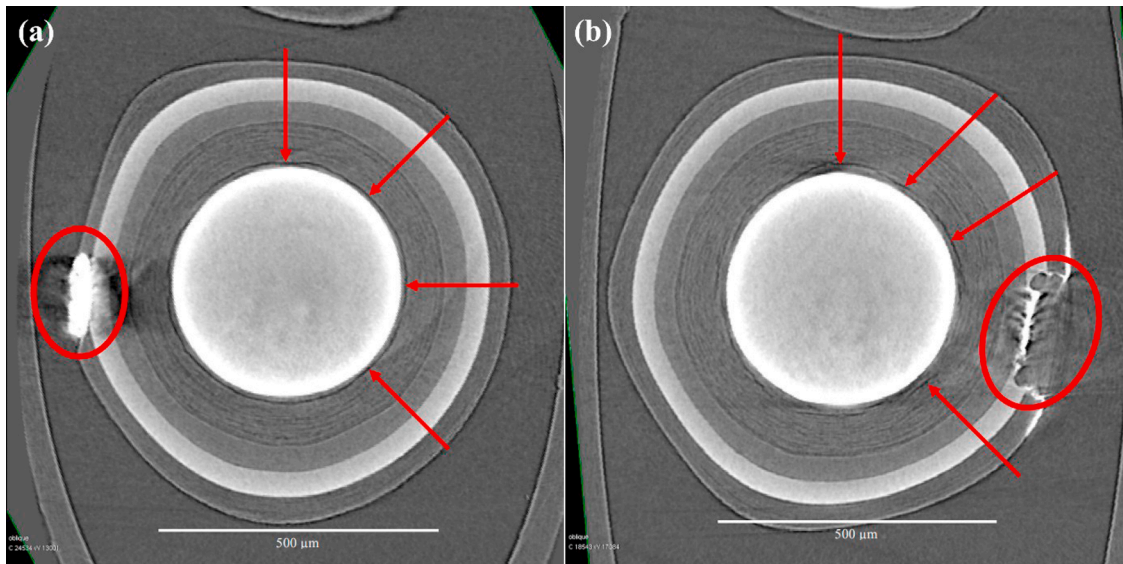


Fig. 9. X-ray microtomography images of defective unirradiated TRISO particles with high-Z elements infiltrations, circled in red. Reproduced from [52]. The red arrows point to the most evident delamination points but, upon closer inspection, the kernel looks completely detached from the buffer, with some residual carbon attached to the kernel, suggesting the crack originated in the buffer itself.

buffer layer would fully debond from the kernel during the final cool-down phase. Going back to Fig. 6, it can be seen that for both the radial and hoop directions that the full decoupling of the kernel and buffer causes an almost complete relaxation of the stress profile. The kernel becomes stress-free, as it is not bonded to any layer with a different thermal expansion coefficient, whereas the remainder of the existing stresses can be associated to the difference in CTE between SiC, buffer and PyC layers. The resulting radial stress profile now shows signs of residual compression in the buffer and OPyC layers, limited to a few MPa. The IPyC and SiC, however, show a varying state of slight radial compression and tension, with a small peak (~20 MPa) of tensile stress at the boundary between IPyC and SiC. Moreover, the hoop stress distribution is more similar to the fully bonded model, although with the kernel showing as stress-free. Also, the compression stress in the SiC layer decreased by almost an order of magnitude to around 90 MPa, whereas the stresses in the PyC layers are comparable to the fully bonded model. This similarity, however, might be associated to the method through which the residual stress distribution has been transposed from one fabrication step to the next one, which is simply to sum the final step stresses from one step onto the initial model of the next

one. Indeed, the adopted strategy assumes the debonding occurs perfectly at the beginning of the final cooldown step (Step 10 in Table 6), which is an arbitrary choice for ease of modelling. An improvement to the model would be to include a stress threshold-based detachable interface, which would make the layers debond when a certain level of tensile radial stress is reached (i.e., 40 to 50 MPa for the buffer and 80 to 150 MPa for the kernel).

The effect of the annealing phase has also been investigated for the debonded model, with the results reported in Fig. 10. The effect on the hoop stresses, especially in the SiC layer is very similar to the ones observed for the fully bonded model, confirming that the variation in the layers' diameters led by thermal creep could help in increasing the pre-compression in the hoop direction. However, it must be noted that radially, the behaviour of the stresses is different, with slight increases towards greater tensile values in the IPyC and SiC layers. As with the fully bonded model, the effect of thermal annealing appears to dwindle to negligibility after 12 h of treatment.

The main result to be highlighted from this analysis is that the residual stresses in the layers are not predicted to be negligible, as so often assumed in literature [39–42]. In fact, they may be comparable to the

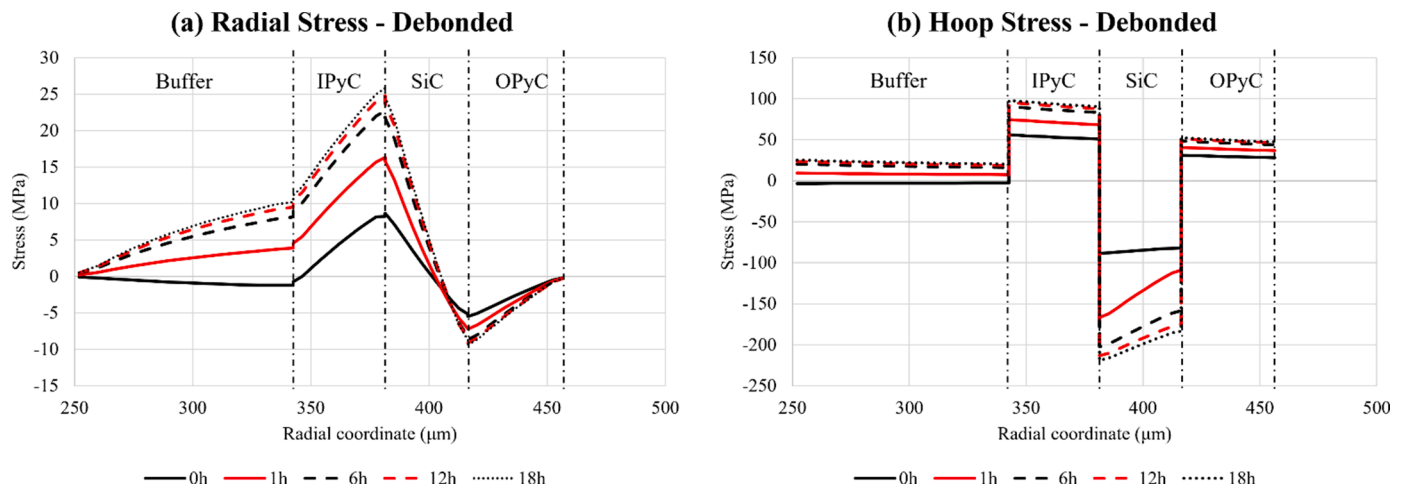


Fig. 10. Effect of different stages of thermal annealing at 1950 °C on the radial (a) and hoop (b) residual stress in German AVR TRISO with debonding of the buffer layer from the kernel. The kernel is stress-free at room temperature in this situation and its stress distribution has been omitted for clarity purposes.

stress changes predicted to arise in the particles during reactor operations [38,39,42]. This appears to be the situation in both the case that the particle's layers have survived the fabrication thermal transients as well as if the kernel has become detached from the buffer. Indeed, if debonding with the SiC layer is avoided during fabrication, then the pyrolytic carbon layers could be under pre-tension in the initial stages of the fuel life. More significantly, however, a state of pre-compression may exist for the SiC layer, which could be beneficial to the overall structural integrity of the particle by resisting the development of tensile stress from increasing fission gas pressure.

Although this analysis is focused on unirradiated TRISO particles, multiple authors in literature [53–55] have often observed large gaps between buffer and IPyC layers in irradiated TRISO particles. This effect is related to the effect of irradiation on buffer pyrolytic carbon, which experimentally has been proven to shrink (the densification effect observed in [54]) and therefore debond from the IPyC. Indeed, IPyC has a much lower porosity compared to the buffer (as shown in Table 1) which will make it less affected by densification, and a higher elastic modulus, which will cause it to struggle to follow the irradiation strain experienced by the buffer. To confirm that such a debonding scenario would be more likely related to the reactor operation phase in TRISO lifetime, a set of simulations studying a fabrication model with buffer-IPyC debonding has been run. These preliminary simulations produced residual radial stresses in the kernel and buffer that were higher than those predicted in the previous model to cause kernel-buffer debonding, and thus kernel-buffer debonding would still be expected to occur first to relieve stress in fabrication in preference to buffer-IPyC debonding.

3.3. Ovality/Defect analysis

In view of the high degree of ovality existing in many of the available micrographs of real TRISO particles [52,56], and in the wake of other works published discussing the effect of ovality or defects on the performance of TRISO in reactor [41,57,58], an additional set of simulations was performed to understand the effect of “flat spots” on the residual stress distribution of TRISO particles.

The model assumes a manufacturing defect has occurred in the deposition of the buffer layer, which is arguably the one more susceptible to thickness variation due to its overall greater dimension and faster deposition rate, as shown in Table 2. To gain a good insight into this peculiar ovality effect, the model has been flattened so as to form a 30° wide “flat spot”, shown in Fig. 11. In the 3D reconstruction of the axial-symmetric model this would mean a cone of 30° overture, which is

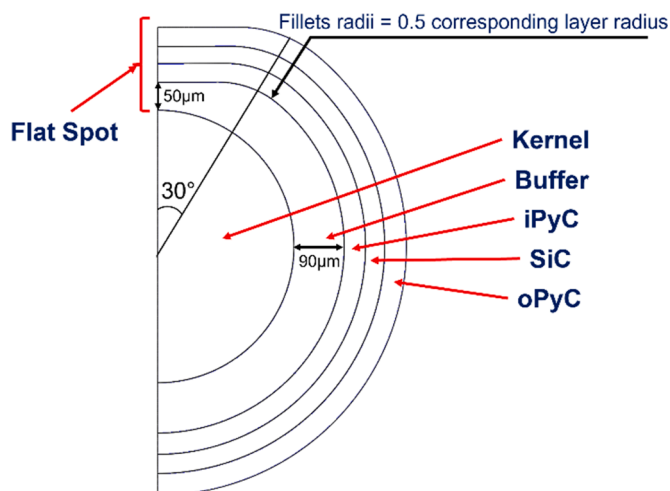


Fig. 11. Representation of the axial-symmetric model adopted for the ovality analysis.

connected to the spherical shape through “fillets” with radii corresponding to half the radius of the respective interface. Results for the ovality study are related to a model with debonding between kernel and buffer, therefore these will be compared to the debonded spherical model only.

The comparison shown in Fig. 12 is related to the flattened model shown in Fig. 11, where the rest of the boundary conditions and model parameters have been left unchanged.

Figure 12a shows a change in the trend of the radial stresses, which are predicted to be completely compressive but no more than 4 MPa in magnitude in the “flat spot”. This is probably related to the deformation led by the spherical kernel (in the radial direction) and the rest of the spherical part of the layers (in the hoop direction). The spherical part of the particle tends to shrink more than the “flat spot”, hence when the temperature is dropped, the spherical parts tend to “pull” the “flat spot” in, leading to an overall radial compression state. The behaviour of radial stress in the middle of the “fillet” between the spherical and flattened region shows an overall increase in the absolute values of stress in all the layers.

Figure 12b shows that hoop stresses are predicted to be much greater in magnitude than the radial stresses shown in Fig. 12a. The hoop stress in the “fillet” follows the same trend as that of the spherical results, albeit with an increased stress gradient especially in the SiC layer, resulting in higher values of compression at the interface with the IPyC layer (advantageous for resisting pressurisation by fission gas) and lower at the interface with OPyC. As for the spherical results, this would not necessarily affect negatively the behaviour of the particle, as a state of pre-compression is desirable to counteract the tensile stresses arising during the pressurisation of the particle due to the gaseous fission products released from the kernel.

The “flat spot” behaviour shows overall increased stresses in both PyC layers and the SiC layer, but with opposite trends from the inside towards the outside of the layers. The change in trend leads to a small decrease in the compressive residual stress in the SiC layer at the crucial interface between IPyC and SiC, which is in effect the wall of the particle, as a pressure vessel containing fission gases. As a result, this could affect the particle's ability to resist rising tensile hoop stress due to fission gas pressure and lead to a greater risk of failure due to crack propagation from this interface through the SiC layer. The explanation for such a difference could be related to the effect of different shapes being coupled, which would affect the magnitude of the strains, with the spherical part straining differently and therefore driving or being driven by the flattened spot to a different stress distribution. However, it is difficult to determine a single or multiple cause for the difference as there are several materials contributing to the final distribution, with creep also possibly affecting the results.

It is important to notice that the stress profile at the centre of the “flat spot” is an extreme situation, likely not representative of the average behaviour of ovalised TRISO particles. However, it is a good example to understand the impact of such a commonly observed defect on the residual stress state of TRISO particle, and possibly to infer on the reasons why interface failure may occur during the reactor transients.

4. Conclusions

The work detailed in this paper produced several distributions of residual stresses deriving from the fabrication procedure of TRISO particles:

- The residual stress analysis in a model with no debonding predicted implausibly highly tensile stresses in the radial direction while the hoop stress distribution was characterised by tensile stress in the kernel, IPyC and OPyC layers, and compressive stress in the buffer but foremost in the SiC layer.
- The model with debonding of the kernel-buffer interface resulted in an evident relaxation of the stress profile compared to the fully

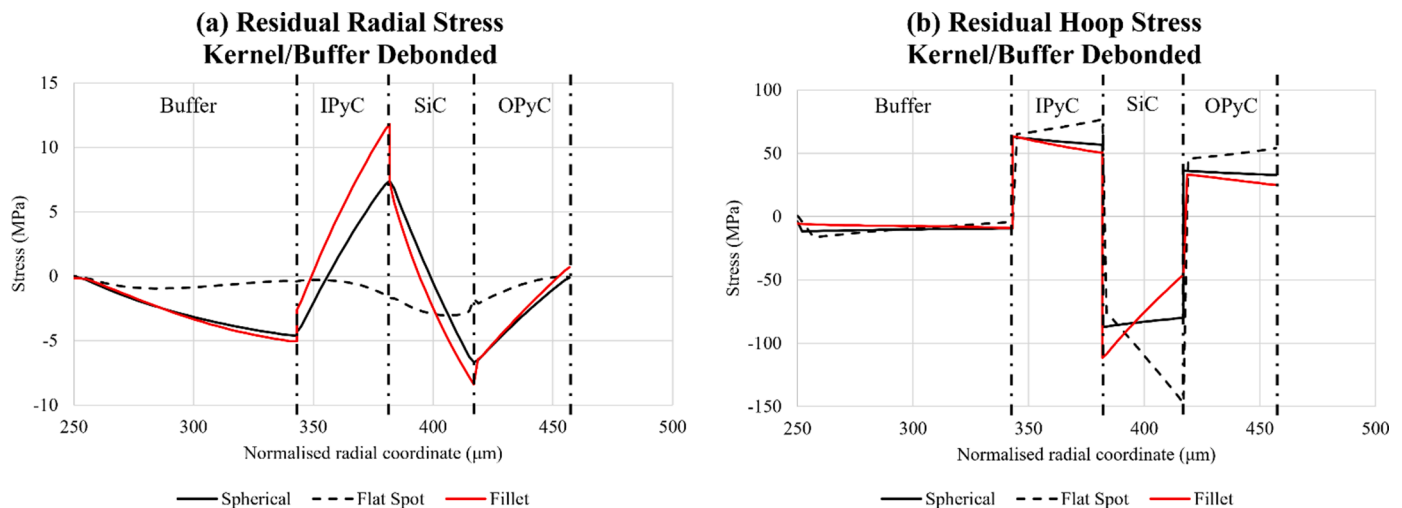


Fig. 12. Comparison between spherical and anomalous residual stress profiles, for a model with kernel-buffer debonding. The “flat spot” distribution is taken from the middle of the flat surface shown in Fig. 11, whereas the “fillet” is taken from the middle of the junction between the spherical and the flattened surface. The radial coordinates begin from the buffer (250 μm) as the kernel resulted stress-free in both directions and over the whole model. The radial coordinates for the “flat spot” and “fillet” distributions have been normalised to the spherical model radial coordinates for ease of comparison.

bonded case. This is characterised by an effective release of all stress in the kernel and a major reduction of both radial and hoop stresses in the surrounding layers (e.g., 90 MPa compressive hoop stress in SiC). Such values are more reasonable compared to the fully bonded model. This suggests that due to the high thermal strains experienced by the particle during the fabrication process, the most likely outcome is the separation of the buffer layer from the kernel.

- Thermal ageing significantly also increases the desirable compressive stress in the SiC layer in the crucial hoop direction (when considered as a vessel for fission gas pressure), albeit with a slight increase in tensile stress in the radial direction.
- Modelling the inclusion of ovality of the particle, with the buffer layer detached from the kernel, showed a difference in the stress profiles between a “flat spot” and the spherical results. The hoop stress distribution in the “flat spot” is similar to the spherical results albeit with an opposite hoop stress radial gradient in each of the layers. This leads to a slight magnification of the peak values of stress in the PyC layer, but most importantly, it leads to changes in the SiC layer stress profile, with a decrease of the compressive residual stress at the interface between the IPyC and SiC layers. This could present a weak point which is less able to resist rising tensile stress due to fission gas pressure.

Although the results reported in the paper are specific to one type of particle, these findings should move the TRISO fuel performance modelling community towards considering the effect that residual stresses present at the end of the fabrication sequence could have on the behaviour of the particles in-reactor. This may increase the validity of TRISO as an advanced technology fuel choice and at the same time it could highlight new areas of research aimed at optimising the production sequence of the particle to maximise the positive effects (such as the SiC hoop pre-compression) and minimise the undesirable ones (tension in the PyC layers).

CRediT authorship contribution statement

Angelo Battistini: Conceptualization, Methodology, Software, Investigation, Writing – original draft, Writing – review & editing, Visualization, Validation, Data curation, Formal analysis. **Thomas A. Haynes:** Supervision, Writing – review & editing, Software. **Daniel Shepherd:** Supervision, Writing – review & editing. **Mark R. Wenman:** Conceptualization, Supervision, Writing – review & editing, Resources,

Funding acquisition, Project administration.

Declaration of Competing Interest

The authors declare the following financial interests/personal relationships which may be considered as potential competing interests:

Angelo Battistini reports financial support was provided by National Nuclear Laboratory Ltd. Thomas A. Haynes reports financial support was provided by National Nuclear Laboratory Ltd. Mark R. Wenman reports financial support was provided by National Nuclear Laboratory Ltd. Daniel Shepherd reports financial support was provided by National Nuclear Laboratory Ltd. Angelo Battistini reports financial support was provided by UK Research and Innovation. Thomas A. Haynes reports financial support was provided by UK Research and Innovation. Mark R. Wenman reports financial support was provided by UK Research and Innovation. Angelo Battistini reports financial support was provided by United Kingdom Department for Business Energy and Industrial Strategy. Thomas A. Haynes reports financial support was provided by United Kingdom Department for Business Energy and Industrial Strategy. Mark R. Wenman reports financial support was provided by United Kingdom Department for Business Energy and Industrial Strategy. Angelo Battistini reports financial support was provided by Engineering and Physical Sciences Research Council. Thomas A. Haynes reports financial support was provided by Engineering and Physical Sciences Research Council. Mark R. Wenman reports financial support was provided by Engineering and Physical Sciences Research Council. Daniel Shepherd reports a relationship with National Nuclear Laboratory Ltd that includes: employment. Thomas A. Haynes reports a relationship with University of East Anglia that includes: employment. Thomas A. Haynes reports a relationship with Imperial College London that includes: associate lecturer.

Data availability

Data will be made available on request.

Acknowledgements

This work was funded under the £46 m Advanced Fuel Cycle Programme as part of the Department for Business, Energy, and Industrial Strategy’s (BEIS) £505 m Energy Innovation Programme, and the Centre

for Doctoral Training Nuclear Energy Futures, under the UKRI grant EP/S023844/1.

References

- [1] M.S.T. Price, The Dragon Project origins, achievements and legacies, Nucl. Eng. Des. 251 (2012) 60–68, <https://doi.org/10.1016/j.nucengdes.2011.12.024>. Oct.
- [2] State-of-the-Art Report on Light Water Reactor Accident-Tolerant Fuels. Nuclear energy agency - organisation for economic co-operation and development, 2018.
- [3] S.J. Zinkle, K.A. Terrani, J.C. Gehin, L.J. Ott, L.L. Snead, Accident tolerant fuels for LWRs: a perspective, J. Nucl. Mater. 448 (1–3) (2014), <https://doi.org/10.1016/j.jnucmat.2013.12.005>.
- [4] R.L. Seibert, B.C. Jolly, M. Balooch, D.P. Schappel, K.A. Terrani, Production and characterization of TRISO fuel particles with multilayered SiC, J. Nucl. Mater. 515 (2019) 215–226, <https://doi.org/10.1016/j.jnucmat.2018.12.024>. Mar.
- [5] W.F. Skerjanc, J.T. Maki, B.P. Collin, D.A. Petti, Evaluation of design parameters for TRISO-coated fuel particles to establish manufacturing critical limits using PARFUME, J. Nucl. Mater. 469 (2016) 99–105, <https://doi.org/10.1016/j.jnucmat.2015.11.027>.
- [6] T.J. Gerczak, J.D. Hunn, R.A. Lowden, T.R. Allen, SiC layer microstructure in AGR-1 and AGR-2 TRISO fuel particles and the influence of its variation on the effective diffusion of key fission products, J. Nucl. Mater. 480 (2016), <https://doi.org/10.1016/j.jnucmat.2016.08.011>.
- [7] P. Demange, J. Marian, M. Caro, A. Caro, TRISO-fuel element thermo-mechanical performance modeling for the hybrid LIFE engine with Pu fuel blanket, J. Nucl. Mater. 405 (2) (2010) 144–155, <https://doi.org/10.1016/j.jnucmat.2010.08.004>.
- [8] J.M. Beck and L.F. Pincock, “High temperature gas-cooled reactors lessons learned applicable to the next generation nuclear plant,” Apr. 2011. doi: 10.2172/1023461.
- [9] M. Lang, H. Xie, Y. Dong, Three design basis accidents’ analysis on the HTR-10GT, Sci. Technol. Nucl. Install. 2017 (2017) 1–13, <https://doi.org/10.1155/2017/1686291>.
- [10] S. Hamamoto, et al., Improving the safety of the high temperature gas-cooled reactor ‘HTTR’ based on Japan’s new regulatory requirements, Nucl. Eng. Des. 388 (2022), 111642, <https://doi.org/10.1016/j.nucengdes.2021.111642>. Mar.
- [11] D.A. Copping and D.L. Moses, “Fort Saint Vrain gas cooled reactor operational experience - ORNL/TM-2003/223,” 2003.
- [12] E. Blandford, et al., Kairos power thermal hydraulics research and development, Nucl. Eng. Des. 364 (2020), 110636, <https://doi.org/10.1016/j.nucengdes.2020.110636>. Aug.
- [13] T.A. Haynes, M.R. Wenman, and D. Shepherd, “TRISO particle fuel brief literature review material properties,” 2021.
- [14] Framatome, “Framatome’s HTGR: industrial process heat, Hydrogen, electricity.” https://www.framatome.com/EN/us_platform-3225/framatome-htr.html.
- [15] Z. Zhang, et al., The Shandong Shidao Bay 200 MWe high-temperature gas-cooled reactor pebble-bed module (HTR-PM) demonstration power plant: an engineering and technological innovation, Engineering 2 (1) (2016) 112–118, <https://doi.org/10.1016/j.eng.2016.01.020>. Mar.
- [16] Y. Brits, F. Botha, H. van Antwerpen, H.-W. Chi, A control approach investigation of the Xe-100 plant to perform load following within the operational range of 100–25–100%, Nucl. Eng. Des., vol. 329 (2018) 12–19, <https://doi.org/10.1016/j.nucengdes.2017.11.041>. Apr.
- [17] P.A. Demkowicz, D.A. Petti, K. Sawa, J.T. Maki, R.R. Hobbins, TRISO-coated particle fuel fabrication and performance,” Comprehensive Nuclear Materials, Elsevier, 2020, pp. 256–333.
- [18] Office of Nuclear Regulatory Research, “TRISO-coated particle fuel phenomenon identification and ranking tables (PIRTs) for fission product transport due to manufacturing, operations, and accidents,” Washington DC, 2004.
- [19] IAEA, “High temperature gas cooled reactor fuels and materials,” 2010. [Online]. Available: https://www-pub.iaea.org/MTCD/Publications/PDF/TE_1645_CD/PDF/TECD0C_1645.pdf.
- [20] J. Wang, An Integrated Performance Model for High Temperature Gas Cooled Reactor Coated Particle Fuel, Massachusetts Institute of Technology, 2004.
- [21] D.A. Petti, J.T. Maki, J. Buongiorno, and R.R. Hobbins, “Key differences in the fabrication, irradiation, and safety testing of U.S. and German TRISO-coated particle fuel and their implications on fuel performance.” INEEL/EXT-02-00300, Jun. 2002, doi: 10.2172/910651.
- [22] L.J. Siefken, E.W. Coryell, E.A. Harvego, J.K. Hohorst, MATPRO - A Library of Materials Properties for Light-Water-Reactor Accident Analysis, Idaho National Engineering and Environmental Laboratory, 2001. NUREG/CR-6150, Vol. 4, Rev. 2 - INEL-96/0422[Online]. Available, <https://www.nrc.gov/docs/ML0103/ML010330363.pdf>.
- [23] D.A. Petti, P. Martin, M. Phélip, Development of Improved Models and Designs for Coated-Particle Gas Reactor Fuels, Idaho National Laboratory, 2002. INEEL/EXT-02-01493, November.
- [24] R.L. COBLE, W.D. KINGERY, Effect of porosity on physical properties of sintered alumina, J. Am. Ceram. Soc. 39 (11) (1956) 377–385, <https://doi.org/10.1111/j.1151-2916.1956.tb15608.x>. Nov.
- [25] K.H. Park, J.Y. Park, J.H. Park, W.J. Kim, C.H. Jung, and Y.W. Lee, “A novel approach to the porosity evaluation of pyrolytic carbon layers in TRISO-coated fuel,” Accessed: Mar. 10, 2023. [Online]. Available: https://inis.iaea.org/search/search.aspx?orig_q=RN:37096488.
- [26] J.J. Powers, B.D. Wirth, A review of TRISO fuel performance models, J. Nucl. Mater. 405 (1) (2010) 74–82, <https://doi.org/10.1016/j.jnucmat.2010.07.030>.
- [27] T.A. Haynes, et al., Peridynamic modelling of cracking in TRISO particles for high temperature reactors, Engrxiv (2022), <https://doi.org/10.31224/2635>.
- [28] R. Li, B. Liu, C. Tang, Modification in the stress calculation of PyC material properties in TRISO fuel particles under irradiation, J. Nucl. Sci. Technol. 54 (7) (2017) 752–760, <https://doi.org/10.1080/00223131.2017.1309304>. Jul.
- [29] L.L. Snead, T. Nozawa, Y. Katoh, T.-S. Byun, S. Kondo, D.A. Petti, Handbook of SiC properties for fuel performance modeling, J. Nucl. Mater. 371 (1–3) (2007) 329–377, <https://doi.org/10.1016/j.jnucmat.2007.05.016>. Sep.
- [30] S.G. Popov, V.K. Ivanov, J.J. Carbajo, G.L. Yoder, Thermophysical Properties of MOx and UO₂ Fuels Including the Effects of Irradiation, Oak Ridge National Laboratory, 2000. ORNL/TM-2000/351.
- [31] A.I. Savvatimskiy, Measurements of the melting point of graphite and the properties of liquid carbon (a review for 1963–2003), Carbon N. Y. 43 (6) (2005) 1115–1142, <https://doi.org/10.1016/j.carbon.2004.12.027>. May.
- [32] J.K. Fink, M.G. Chasanov, L. Leibowitz, Thermophysical properties of uranium dioxide, J. Nucl. Mater. 102 (1–2) (1981) 17–25, [https://doi.org/10.1016/0022-3115\(81\)90541-9](https://doi.org/10.1016/0022-3115(81)90541-9). Nov.
- [33] E. López-Honorato, C. Chiritescu, P. Xiao, D.G. Cahill, G. Marsh, T.J. Abram, Thermal conductivity mapping of pyrolytic carbon and silicon carbide coatings on simulated fuel particles by time-domain thermoreflectance, J. Nucl. Mater. 378 (1) (2008) 35–39, <https://doi.org/10.1016/j.jnucmat.2008.04.007>. Aug.
- [34] M.J. Kania, H. Nabielek, H. Nickel, Coated particle fuels for high-temperature reactors. Materials Science and Technology, Wiley-VCH Verlag GmbH & Co. KGaA, Weinheim, Germany, 2015, pp. 1–183.
- [35] H. Nabielek, G. Kaiser, H. Huschka, H. Ragos, M. Wimmers, W. Theymann, Fuel for pebble-bed HTRs, Nucl. Eng. Des. 78 (2) (1984) 155–166, [https://doi.org/10.1016/0029-5493\(84\)90301-7](https://doi.org/10.1016/0029-5493(84)90301-7). Apr.
- [36] K. Minato, K. Fukuda, Thermodynamic analysis of behaviour of HTGR fuel and fission products under accidental air or water ingress conditions, Int. Atomic Energy Agency (IAEA) (1995) [Online]. Available, http://inis.iaea.org/search/search.aspx?orig_q=RN:26045237.
- [37] American Nuclear Society, China’s First High-Temperature Reactor Goes Critical, Nuclear News (2001) 34–35. Feb.
- [38] D.G. Martin, Considerations pertaining to the achievement of high burn-ups in HTR fuel, Nucl. Eng. Des. 213 (2–3) (2002) 241–258, [https://doi.org/10.1016/S0029-5493\(01\)00502-7](https://doi.org/10.1016/S0029-5493(01)00502-7).
- [39] G.K. Miller, R.G. Bennett, Analytical solution for stresses in TRISO-coated particles, J. Nucl. Mater. 206 (1) (1993) 35–49, [https://doi.org/10.1016/0022-3115\(93\)90230-V](https://doi.org/10.1016/0022-3115(93)90230-V). Nov.
- [40] G.K. Miller, D.A. Petti, J.T. Maki, D.L. Knudson, PARFUME Theory and Model Basis Report, Idaho National Laboratory, 2018. INL/EXT-08-14497 - September.
- [41] G.K. Miller, D.A. Petti, J.T. Maki, Consideration of the effects of partial debonding of the IPyC and particle asphericity on TRISO-coated fuel behavior, J. Nucl. Mater. 334 (2–3) (2004) 79–89, <https://doi.org/10.1016/j.jnucmat.2004.04.330>. Sep.
- [42] D. Schappel, K.A. Terrani, Stress profile in coating layers of TRISO fuel particles in contact with one another, Nucl. Sci. Eng. 196 (11) (2022) 1349–1360, <https://doi.org/10.1080/00295639.2022.2090214>. Nov.
- [43] A. Leide, X-Ray Tomography of TRISO particles, (Personal Communication) (2022).
- [44] J.D. Hales, et al., BISON Theory Manual the Equations Behind Nuclear Fuel Analysis, Idaho National Laboratory, 2016, <https://doi.org/10.2172/1374503>. INL/EXT-13-29930 Rev. 3, Sep.
- [45] T.A. Haynes, “Finite Element Modelling of Nuclear Fuel Performance in Advanced Gas-Cooled Reactors,” Pages 186, 203, Imperial College London.
- [46] C.H. CARTER, R.F. DAVIS, J. BENTLEY, Kinetics and mechanisms of high-temperature creep in silicon carbide: II, chemically vapor deposited, J. Am. Ceram. Soc. 67 (11) (1984) 732–740, <https://doi.org/10.1111/j.1151-2916.1984.tb19510.x>. Nov.
- [47] W.R. Cannon, T.G. Langdon, Creep of ceramics, J. Mater. Sci. 23 (1) (1988) 1–20, <https://doi.org/10.1007/BF01174028>. Jan.
- [48] R. Kirchofer, J.D. Hunn, P.A. Demkowicz, J.I. Cole, B.P. Gorman, Microstructure of TRISO coated particles from the AGR-1 experiment: SiC grain size and grain boundary character, J. Nucl. Mater. 432 (1–3) (2013) 127–134, <https://doi.org/10.1016/j.jnucmat.2012.08.052>. Jan.
- [49] K. Bongartz, E. Gyarmati, H. Schuster, K. Täuber, The brittle ring test: a method for measuring strength and young’s modulus on coatings of HTR fuel particles, J. Nucl. Mater. 62 (2–3) (1976) 123–137, [https://doi.org/10.1016/0022-3115\(76\)90012-X](https://doi.org/10.1016/0022-3115(76)90012-X).
- [50] K.C. Radford, Effect of fabrication parameters and microstructure on the mechanical strength of UO₂ fuel pellets, J. Nucl. Mater. 84 (1–2) (1979) 222–236, [https://doi.org/10.1016/0022-3115\(79\)90165-X](https://doi.org/10.1016/0022-3115(79)90165-X). Oct.
- [51] M. Oguma, Cracking and relocation behavior of nuclear fuel pellets during rise to power, Nucl. Eng. Des. 76 (1) (1983) 35–45, [https://doi.org/10.1016/0029-5493\(83\)90045-6](https://doi.org/10.1016/0029-5493(83)90045-6). Oct.
- [52] G.W. Helmreich, J.D. Hunn, D.J. Skitt, J.A. Dyer, and A.T. Schumacher, “X-ray analysis of defects and anomalies in AGR-5/6/7 TRISO Particles - ORNL/TM-2017/038,” 2017.
- [53] D. Schappel, G. Pastore, K.A. Terrani, Modeling interface debonding in coated fuel particles with BISON, Nucl. Sci. Eng. 196 (3) (2022) 276–284, <https://doi.org/10.1080/00295639.2021.1955590>. Mar.
- [54] S.A. Ploger, P.A. Demkowicz, J.D. Hunn, J.S. Kehn, Microscopic analysis of irradiated AGR-1 coated particle fuel compacts, Nucl. Eng. Des. 271 (2014) 221–230, <https://doi.org/10.1016/j.nucengdes.2013.11.036>. May.
- [55] P.A. Demkowicz, J.D. Hunn, D.A. Petti, R.N. Morris, Key results from irradiation and post-irradiation examination of AGR-1 UCO TRISO fuel, Nucl. Eng. Des. 329 (2018) 102–109, <https://doi.org/10.1016/j.nucengdes.2017.09.005>. Apr.

- [56] J. Phillips, E. Shaber, Compact Process Development at Babcock, Idaho National Laboratory, 2012, pp. 15–18, rev 0INL/EXT-11-23166, March.
- [57] J.D. Hales, R.L. Williamson, S.R. Novascone, D.M. Perez, B.W. Spencer, G. Pastore, Multidimensional multiphysics simulation of TRISO particle fuel, *J. Nucl. Mater.* 443 (1–3) (2013) 531–543, <https://doi.org/10.1016/j.jnucmat.2013.07.070>. Nov.
- [58] D.A. Petti, J. Buongiorno, J.T. Maki, R.R. Hobbins, G.K. Miller, Key differences in the fabrication, irradiation and high temperature accident testing of US and German TRISO-coated particle fuel, and their implications on fuel performance, *Nucl. Eng. Des.* 222 (2–3) (2003) 281–297, [https://doi.org/10.1016/S0029-5493\(03\)00033-5](https://doi.org/10.1016/S0029-5493(03)00033-5). Jun.